Published in final edited form as:
Dev Biol. 2011 February 15; 350(2): 311–322. doi:10.1016/j.ydbio.2010.11.033.

Regulation of Mouse Oocyte Microtubule and Organelle Dynamics by PADI6 and the Cytoplasmic Lattices

Rui Kan[1], **Piraye Yurttas**[1,2], **Boram Kim**[1], **Mei Jin**[1], **Luccie Wo**[3], **Bora Lee**[4], **Roger Gosden**[4], and **Scott A. Coonrod**[1,*]

[1] Baker Institute for Animal Health, Cornell University, Ithaca, NY 14853, USA

[2] Celmatix, Inc., Hubert Street, New York, NY 10013, USA

[3] Department of Biomedical Engineering, Johns Hopkins University, Baltimore, MD 21218, USA

[4] Center for Reproductive Medicine and Infertility, Weill Cornell Medical College, New York, NY 10065, USA

Abstract

Organelle positioning and movement in oocytes is largely mediated by microtubules (MTs) and their associated motor proteins. While yet to be studied in germ cells, cargo trafficking in somatic cells is also facilitated by specific recognition of acetylated MTs by motor proteins. We have previously shown that oocyte-restricted PADI6 is essential for formation of a novel oocyte-restricted fibrous structure, the cytoplasmic lattices (CPLs). Here, we show that α-tubulin appears to be associated with the PADI6/CPL complex. Next, we demonstrate that organelle positioning and redistribution is defective in PADI6-null oocytes and that alteration of MT polymerization or MT motor activity does not induce organelle redistribution in these oocytes. Finally, we report that levels of acetylated microtubules are dramatically suppressed in the cytoplasm of PADI6-null oocytes, suggesting that the observed organelle redistribution failure is due to defects in stable cytoplasmic MTs. These results demonstrate that the PADI6/CPL superstructure plays a key role in regulating MT-mediated organelle positioning and movement.

Keywords

Cytoplasmic lattice; PADI6; Tubulin; Acetylated microtubule; Spindle; Organelle redistribution; Endoplasmic reticulum; Mitochondria; Oocyte maturation

Introduction

While the role of MTs and associated motor proteins in non-mammalian oocyte and early embryonic development is well documented (Elinson and Rowning, 1988; Gard, 1991; Lane and Allan, 1999; Lessman, 1987; Schroeder and Gard, 1992; Yisraeli et al., 1990), less is known about the MT network during early mammalian development. However, several mouse studies have shown that MT are required for formation of MT organizing centers and the meiotic spindle apparatus, polar body extrusion, pronuclear migration, and mitotic

* Correspondence should be addressed to: Scott A. Coonrod Baker Institute for Animal Health, Cornell University, Hungerford Hill Road, Ithaca, NY 14853, USA, Phone: (607) 256-5657, Fax: (607) 256-5608, sac269@cornell.edu.

spindle formation in early embryos (Calarco-Gillam et al., 1983; Maro et al., 1990; Maro and Verlhac, 2002; Schatten et al., 1985) More recently, oocyte MTs have also been found to drive endoplasmic reticulum (ER) and mitochondrial re-targeting during oocyte maturation (FitzHarris et al., 2007; Mehlmann et al., 1995; Van Blerkom, 1991; Van Blerkom and Runner, 1984).

MT mediated organelle transport is facilitated by molecular motor proteins such as the kinesins, which move along the MT from the minus end to the plus end, and dynein, which moves in the opposite direction(Hirokawa et al., 1998). Regulation of ATP-ase dependent motor activity is mediated by a wide range of factors including MT-associated proteins, cell cycle regulatory factors, and, more recently, tubulin acetylation(Hammond et al., 2008). In somatic cells, tubulin acetylation specifically occurs on lysine 40 of alpha tubulin following MT assembly and this post-translational modification was previously documented to be abundantly represented in stable microtubules(Barlan and Gelfand, 2010). Interestingly, tubulin acetylation has also recently been found by several groups to play a critical role in the trafficking of cellular cargo by both dynein and by kinesin (Cambray-Deakin et al., 1988; Chen et al., 2010; Friedman et al., 2010). In mammalian oocytes, acetylated tubulin has also previously been associated with stable microtubules at the spindle poles, however, a potential role in cytoplasmic organelle redistribution has not been previously investigated(Schatten et al., 1985).

We have previously characterized a novel maternal effect gene, peptidylarginine deiminase 6 (PADI6), and found that this oocyte-and early embryo-restricted protein localizes to (Wright et al., 2003), and is required for the formation of, the cytoplasmic lattices (CPLs), a highly abundant poorly-defined structure that is unique to mammalian oocytes and preimplantaion embryos (Esposito et al., 2007). Additionally, we found that the PADI6/CPLs complex appear to contain ribosomal components and to play a role in embryonic genome activation (Yurttas et al., 2008). Recently, we carried out a non-biased Triton X-100 differential solubility screen of wild-type and *Padi6*-null oocytes to identify other CPL-associated factors and found that α-tubulin also seems to be associated with the lattices.

In this report we have tested this hypothesis and present experimental evidence indicating that tubulin associates with PADI6 at the CPLs. Further, we also show that loss of the PADI6/CPL superstructure in *Padi6*-null mice significantly affects ER and mitochondrial positioning, and organelle reorganization during maturation. Next, through use of drugs that alter MT stability and MT motor activity, we show that the ER and mitochondria appear to be “disconnected” from MTs in PADI6-null oocytes. Finally we provide mechanistic insight to these results by showing that levels of acetylated tubulin are severely depleted in PADI6-null oocytes. These findings indicate that the oocyte PADI6/CPL superstructure has a much broader function than previously realized in that they appear to be directly involved in facilitating key MT-mediated events during mammalian oogenesis.

Results and Discussion

α-Tubulin Co-localizes with PADI6 at the Oocyte CPLs

We have previously shown by immuno-EM that PADI6 primarily localizes to the oocyte CPLs and thus can be utilized as a marker for this structure (Wright et al 2003). To begin testing the hypothesis that the CPLs contain tubulin, we first utilized double immunofluoresence (IIF) labeling procedures using antibodies against PADI6 and α-tubulin and confocal microscopy to test whether α-tubulin and PADI6 co-localized in oocytes and early embryos. Results showed that α-tubulin and PADI6 co-localized throughout much of the cytoplasm and the cortex of mouse oocytes and early embryos (Fig. 1A and S1A). As a control, staining was not observed when oocytes were incubated with similar concentrations

of either guinea pig or mouse IgG (Fig. S1D-E).We then used the ZEN 2007 LSM 510 co-localization software package to further quantify the degree of co-localization and found that the Manders' overlap coefficient for co-localization of α-tubulin and PADI6 in the oocyte cytoplasm was 0.94 and Pearson's correlation coefficient R for the co-localization was 0.90. While PADI6 and α-tubulin co-localized throughout much of the cytoplasm, PADI6 staining was not observed on MTs at the meiotic and mitotic spindles (Figure 1A and S1A, arrows in merge panel of mature oocytes, 2-cell and morulas), suggesting that PADI6 does not associate with α-tubulin at spindle MTs.

While the majority of proteins are extracted from oocytes by Triton X-100, oocyte CPLs are resistant to extraction with this detergent (Gallicano et al., 1991). Therefore, to more directly test whether α-tubulin and PADI6 co-localized at the CPLs, we then investigated the degree of co-localization between these proteins following Triton extraction. Germinal vesicle (GV) stage oocytes were treated with 0.1% Triton in a MT/CPL stabilizing buffer followed by IIF. Interestingly, we found that, in addition to MT-associated α-tubulin, a significant amount of non-MT-associated α-tubulin was retained in the wild type oocyte cytoplasm and this fraction appeared to co-localize with PADI6 following Triton treatment (Figure 1B and S1B, co-localization shown in Figure 1B while quantitative data is shown in scatter plot in Figure S1B and in Table S1. Manders' overlap coefficient: 0.97, Pearson's correlation coefficient R: 0.7). As a control, we then investigated whether DDX6 co-localized with PADI6 following Triton extraction. DDX6 has been previously shown to be abundantly expressed in mouse oocytes (Flemr et al., 2010) and is also Triton insoluble (Minshall and Standart, 2004). Results show that DDX6 (green) distributes throughout the cytoplasm in large aggregates and does not strongly co-localize with PADI6 (red) following extraction (Figure 1B, zoom panel, bottom right). The lack of co-localization between PADI6 and DDX6 suggests that the co-localization of PADI6 and α-tubulin is specific and is not due to the non-specific binding of proteins to the Triton-resistant fraction of the extracted oocyte.This finding provides an initial line of evidence that tubulin may form associations with the PADI6/CPL complex. We also found that the cortical fraction of PADI6 and α-tubulin appears to be largely solubilized by Triton X-100 (arrow in top merged panel, Figure 1B), suggesting that a subset of these two proteins may also exist in a soluble form at the oocyte and early embryonic cortex.

To more directly test whether tubulin and PADI6 interact, we carried out immunoprecipitation analysis of GV stage oocyte extracts using either pre-immune or immune PADI6 antibody-bound beads to pull down complexes and anti-α-tubulin antibodies for immunoblotting (Figure 1C). Results showed that α-tubulin was reactive with an appropriately sized protein (~50 kDa) that was pulled down by the PADI6 immune, but not preimmune antisera. While these results suggest that α-tubulin and PADI6 co-localize and interact, it is possible that they do so at locations other than the CPLs. Therefore, we next carried out co-immuno electron microscopy to investigate whether α-tubulin co-localized with PADI6 at the CPLs. Results showed that both α-tubulin (10nm) and PADI6 (6nm) antibody-coated gold particles localized in close association with each other on CPL fibers, while control antibody-coated gold particles were not reactive with the sections (Figure 1D, right panel). Low (top left) and high (bottom left) magnification images of the lattices are included as a reference. Taken together these results suggest that tubulin interacts with PADI6 and is also a component of the oocyte CPLs.

Ultra-structural studies have found that CPLs are conserved amongst a range of mammalian species including humans (Gallicano et al., 1992). Therefore, to test whether our findings in the mouse may be relevant to human oocytes, we investigated whether α-tubulin and PADI6 also co-localized in the cytoplasm of mature human oocytes using confocal microscopy (Figure S1C). Results confirmed that α-tubulin and PADI6 co-localization patterns in human

oocytes were remarkably similar to those of mouse oocytes, supporting the existence and role of a tubulin-containing PADI6/CPL complex in human oocytes.

α-Tubulin Solubility Is Increased in *Padi6*-null Oocytes and Embryos

In previous reports (Kim et al., 2010; Yurttas et al., 2008), we have found that the Triton solubility of CPL-associated proteins is greatly enhanced in mutant oocytes which lack CPLs. This is presumably due to the fact that, in the absence of lattices, CPL-associated proteins do not incorporate into the Triton insoluble structure and are thus more soluble. Therefore, to further test whether tubulin is a component of the oocyte PADI6/CPL complex, we next investigated α-tubulin solubility in wild-type and *Padi6*-null oocytes and embryos following Triton extraction (Figure 1E-G). As a control, we first compared the localization and levels of α-tubulin in non-extracted oocytes and found little difference between wild-type and *Padi6*-null oocytes (Figure 1E, top). Strikingly, however, while non-MT-associated α-tubulin was retained in the cytoplasm of wild-type oocytes following Triton extraction, most non-MT-associated α-tubulin was released from the cytoplasm of *Padi6*-deficient oocytes (Figure 1E, bottom). This result was further validated by Western blot analysis of the oocyte pellets following Triton X-100 extraction (Figure 1F). Results showed a dramatic loss of α-tubulin from the insoluble pellet of *Padi6*-null oocytes compared to those in wild-type oocytes. The intensities of insoluble α-tubulin bands in wild-type and *Padi6*-null oocytes were 100.5 and 9.5 units, respectively (Figure 1G). As a control, we then investigated the solubility of beta-actin following Triton extraction by both confocal analyses (Figure S2A) and Western blot analysis (Figure 1F) and found that the solubility of this protein was not strongly affected by the treatment. Similar to GV oocytes, the non-MT-associated tubulin signal was also lost in *Padi6*-null mature oocytes and 2-cell embryos (Figure S2B and S2C). The significant increase of α-tubulin solubility in GV oocytes, mature oocytes, and 2-cell embryos from *Padi6*-null females further supports the hypothesis that tubulin is associated with the CPLs. Interestingly, previous studies have found that oocytes from several non-mammalian species contain a non-MT associated particulate tubulin-containing protein complex that likely functions to as a tubulin reservoir (Lessman and Kim, 2001; Liu and Lessman, 2007). A potential evolutionarily relationship between the CPLs and these tubulin-containing particulate structures is currently being investigated.

Meiotic Spindle MTs Are Altered in *Padi6*-null Oocytes

To better understand the possible downstream consequences of altered tubulin solubility in PADI6-null oocytes, we next investigated spindle MT morphology in live and fixed PADI6-null oocytes (Figure 2A-B). Measurements of the dimensions of the spindle apparatus and chromosome alignment are shown in Figure 2E. We found that spindle MTs were significantly shorter in *Padi6*-null oocytes than those in wild-type oocytes (22.2 ± 6.4 μm, n = 22, vs. 25.4 ± 3.7 μm, n = 35; $P = 0.037$). Additionally, we found that the equatorial spindle diameter in *Padi6* mutant oocytes was wider than in wild-type (15.3 ± 3.9 μm, n = 22 vs. 12.2 ± 2.6 μm, n = 35; $P = 0.003$) and that the diameter of the aligned chromosomes parallel to the equator was significantly wider in *Padi6* mutant oocytes compared to wild-type (13.7 ± 3.0 μm, n = 22 vs. 10.5 ± 2.1 μm, n = 35; $P < 0.0001$). There was no statistical difference in the width of spindle poles and the distance of spindle to cortex between *Padi6* wild-type and mutant females (5.2 ± 2.5 μm, n = 22 vs. 5.0 ± 2.1 μm, n = 35; 10.3 ± 10.6 μm, n = 22 vs. 10.0 ± 7.9 μm, n = 35).

To further investigate meiotic spindle MTs in the absence of PADI6, we probed *Padi6*-null mature oocytes with antibodies to Aurora kinase A (AURKA), an oocyte MT organizing center-associated serine/threonine kinase that is important for regulating chromosome and spindle dynamics during meiosis I progression (Saskova et al., 2008; Swain et al., 2008).

Results showed that AURKA signal intensity on the spindle apparatus was reduced in *Padi6*-null oocytes (Figure 2C). In order to investigate whether abnormal spindle assembly in *Padi6*-null oocytes could lead to defects in chromosome condensation we also probed *Padi6*-null mature oocytes with antibodies to phospho-histone H3 at Ser10 (pH3S10) as this modification is tightly correlated with chromosome condensation and segregation during mouse oocyte meiosis (Swain et al., 2007). Results showed that the histone H3 phosphorylation staining pattern appeared more condensed in *Padi6*-null oocytes compared to wild-type (Figure 2D). Taken together, this confocal data indicates that the spindle MT structure is altered in *Padi6*-null oocytes.

Aberrant ER and Mitochondrial Positioning and Redistribution in *Padi6*-null Oocytes

In mice, oocyte maturation initiates a dramatic MT-mediated reorganization of the ER from a network of dispersed cytoplasmic foci at the GV stage, to a strong concentration of organelles around the nuclear envelope during germinal vesicle break down (GVBD), and finally to a more cortical clustering with concentrations being observed near the spindle in the mature oocyte (FitzHarris et al., 2003, 2007; Mehlmann et al., 1995). To further test the interrelationship between the PADI6/CPL superstructure and MTs, we carried out several experiments examining the effects of loss of PADI6 on organelle positioning and redistribution. We first investigated the distribution of organelles in growing and fully grown milrinone-arrested GV stage oocytes by indirect immunofluorescence confocal microscopy using anti-calreticulin antibodies to stain the ER and anti-Cytochrome C antibodies to stain the mitochondria (Figure 3A and S3A). Consistent with previous reports (FitzHarris et al., 2007; Mehlmann et al., 1995; Van Blerkom, 1991; Van Blerkom and Runner, 1984), in fully grown wild-type oocytes, the ER and mitochondria were organized in aggregates in the cytoplasm with concentrations of these organelles being found to surround the nucleus. Similar localization patterns were also observed in growing wild type oocytes (Figure S3A). In fully grown mutant oocytes, however, the ER and mitochondria were more diffusely organized in smaller foci throughout the cytoplasm and, in the case of mitochondria, concentrations were also found at the oocyte cortex. These results suggest that PADI6 plays an important role in ER and mitochondrial positioning in immature oocytes and that, in the absence of PADI6, organelle distribution becomes more diffuse.

We next investigated whether the PADI6/CPL structure might also play a role in organelle redistribution during oocyte maturation. Wild type and mutant oocytes were collected at 3-hour intervals during meiotic maturation *in vitro* and the fate of DNA, microtubules, ER, and mitochondria was followed using Hoechst 33342, Tubulin Tracker, ER Tracker, and MitoTracker respectively (Figure 3B). These reagents have been shown by others to specifically target the ER and mitochondria, respectively (Hsieh et al., 2008; Ruiz-Meana et al., 2009; Xu et al., 2007). For all experiments, the confocal settings were configured to prevent fluorescence dye “bleed-through”. To validate these settings, oocytes were stained with each dye separately and images were taken using multiple channels. Each fluorescent signal was found to be well resolved from other signals (Figure S4A-B). Following three hours of culture, a thick ring of ER and mitochondria was seen to circumscribe the nuclear envelope in wild type oocytes. Surprisingly, in mutant oocytes, the majority of ER and mitochondria had migrated to, and accumulated at, the oocyte cortex (Figure 3B). After 6 hours of culture, organelle clusters had migrated towards the center in wild type oocytes while the ER and mitochondria of mutant oocytes remained primarily at the oocyte cortex. By 9 hours, in wild type oocytes the ER and mitochondria were more concentrated at the center of the oocyte and a thin band of ER, but not mitochondria, was observed for the first time in wild-type oocytes in the subcortical region. In mutant oocytes, the organelles were still primarily localized to the cortex in large clusters, with no staining being observed at the subcortical region. At 12 hours, the ER and mitochondria of wild type oocytes appeared to

"follow" the MTs and become more concentrated around MI spindle and also formed a thin band at the oocyte subcortex. In mutant oocytes, however, the ER and mitochondria were no longer concentrated at the cortex and had become more evenly distributed throughout the cytoplasm. We next investigated the localization of ER and mitochondria in MII-arrested wild-type and *Padi6*-null oocytes collected from the oviducts at 13 hour post hCG using antibodies against calreticulin, a major calcium binding protein in the lumen of the ER (Tutuncu et al., 2004) and Cytochrome C, a component of the electron transport chain in mitochondria (Pepling et al., 2007) (Figure 3 C). In wild-type oocytes, we found that both the ER and mitochondria remained centrally localized with concentrations near the spindle apparatus. Further, increased levels of cortical ER, but not mitochondria, were also observed. In contrast, in mutant oocytes the foci of ER and mitochondria were more diffusely distributed throughout the cytoplasm and neither the ER nor mitochondria were concentrated at the oocyte subcortex.

In order to more directly investigate organelle dynamics in PADI6-null oocytes, we next carried out time-lapse image analysis of GV stage oocytes that had been stained with mitotracker. Results showed that, in wild type oocytes, mitochondria were clearly seen to aggregate in clumps and along tracks (presumably MT-based) throughout the cytoplasm of GV-stage oocytes with a considerable amount of back and forth "jostling" movements being observed for these aggregates (Movie S1). In mutant GV stage oocytes, however, the mitochondria were diffusely localized throughout the cytoplasm with much less movement being observed (Movie S1). To more specifically evaluate organelle repositioning during oocyte maturation, we also generated time lapse movies of oocytes undergoing GVBD. Given that we could not follow the ER or mitochondria with fluorescent probes over long time periods due to quenching, we followed the movement of lipid droplets over time because aggregates of these organelles can be easily visualized in oocytes by light microscopy (Shubeita et al., 2008). Results showed that, in wild type oocytes, lipid droplets are initially diffusely localized and then begin to form larger aggregates that migrate towards the nucleus and eventually become clustered around the spindle apparatus following GVBD (Movie S2). In null oocytes, however, the lipid droplets are initially localized in clusters throughout the cytoplasm and then are seen to migrate out towards the cortex during GVBD (Movie S2).

To more directly test whether the oocyte CPLs play a role in organelle targeting, we next performed transmission electron microscopy (TEM) morphometric analysis to quantitate levels of mitochondria, ER, and CPLs in ovulated wild-type and *Padi6*-null mature oocytes (mean ± S.D of percentage per oocyte, number of sections or oocytes) (Figure 3D-E). With respect to oocyte CPLs, results showed that, in wild-type mature oocytes, more lattices were observed at the oocyte cortex (10.59 ±2.86%, n=22 vs. 3.53 ± 1.32%, n=4; $P < 0.0001$), when compared to the middle of the oocyte while, as we have shown previously, no CPLs were observed in *Padi6* mutant oocytes (Esposito et al., 2007; Yurttas et al., 2008). With respect to mitochondria, in wild-type mature oocytes more mitochondria localized to the middle of the oocyte when compared to the cortex (3.60 ±1.72%, n=24 vs. 14.25 ± 0.67%, n=3; $P < 0.0001$). However, in *Padi6*-null mature oocytes the mitochondria were more evenly distributed throughout the cytoplasm (6.83 ±1.15%, n=18 vs. 7.76 ± 1.46%, n=8; $P = 0.138$).

Our ER analysis found that, at the TEM level, there was a slight increase in the amount of ER at the cortex of wild type oocytes (6.72 ±8.35%, n=21 vs. 3.84 ± 2.20%, n=3, $P < 0.05$), which may be reflective of the ER aggregates that were observed in the confocal anti-calreticulin images. However, we did not detect a redistribution of the ER by TEM in PADI6-null oocytes, but instead, we observed a significant increase in the total amount of ER (9.17 ± 3.76%, n=3 vs. 23.23 ± 1.85%, n=5, $P < 0.01$). We currently do not understand

why our EM morphometric analysis does not fully correspond with our confocal anti-calreticulin IF data. However, previous EM analysis of the mature oocyte ER found that the network of smooth ER that is seen in both somatic cells and early stage growing oocytes is replaced by large ER vesicles in the mature oocyte (Wassarman and Josefowicz, 1978). Thus, it is possible that the anti-calretculin antibody is not reactive with all forms of ER in the mature oocyte. Additionally, we are also currently investigating why levels of ER are elevated in the cytoplasm of PADI6-null oocytes.

Taken together, our confocal and EM data further support the hypothesis that the PADI6/CPL complex plays an important role in organelle positioning and redistribution during oocyte maturation. Interestingly, the effects of loss of PADI6 on organelle distribution and targeting was penetrant to the point that pooled wild-type and mutant GV stage oocytes could be easily sorted based on their ER and mitochondrial staining patterns. This strong phenotype is in contrast with the *Padi6*-null defect at the spindle, which, while significant, was less pronounced. Based on these observations, we hypothesize that the PADI6/CPL complex is more directly involved in the regulation of cytoplasmic MT function as opposed to spindle MT function. This prediction is supported by our observation that, while PADI6 co-localizes with tubulin throughout much of the cytoplasm, PADI6 appears to be excluded from the spindle MTs. In further support of this prediction, we also found that the localization of gamma tubulin (an MTOC and meiotic spindle maker (Combelles and Albertini, 2001), during maturation does not appear to be greatly affected by the loss of PADI6 (Figure S3B). In light of these observations, and given the strong apparent cytoplasmic MT defects in mutant oocytes, it is possible that the observed *Padi6*-null spindle defects are actually not caused by direct effects on spindle MTs, but instead are mediated by the inability of the spindle to appropriately mature in the context of a cytoplasm that lacks functional oocyte lattices.

MT-mediated Organelle Transport Is Defective in *Padi6*-null Oocytes

Given the above observations, we next decided to more directly evaluate whether the role of the PADI6/CPL complex in organelle positioning and redistribution was dependent upon cytoplasmic MTs. For these experiments wild-type and *Padi6*-null MII-arrested oocytes were treated with DMSO carrier alone (Figure 4A) or DMSO plus taxol (Figure 4B) and the localization of MTs, ER and mitochondria was then evaluated by confocal microscopy. Anti-α-tubulin antibody staining revealed that spindle MTs and cytoplasmic MT asters were greatly increased in both wild-type and *Padi6*-null oocytes, when compared to DMSO treated oocytes (Figure 4B). Regarding the effects of taxol on organelle distribution, live staining results showed that organelles in taxol-treated wild type oocytes were seen to concentrate around the hyperpolymerized spindle MT (arrows in top merged panel, Figure 4B) and strongly co-localize with a subset of cytoplasmic aster MTs (arrows in top merged panel, Figure S4C). However, in taxol-treated *Padi6*-null oocytes, the ER and mitochondria do not undergo MT-mediated redistribution following taxol treatment and remain diffusely localized throughout the cytoplasm (Figure 4B, bottom panels). To further, test whether the observed organelle positioning defects in PADI6-null oocytes involved MTs, we also treated oocytes with two MT depolymerizing agents, nocodozole (Schatten et al., 1985) (Figure 4C) and vinblastine (Lehtonen, 1985) (Figure 4D) and evaluated the effects of these drugs on mitochondrial localization in wild type and PADI6-null oocytes using MitoTracker. Results showed that, while both reagents effectively depolymerized MTs (as seen by the absence of tubulin tracker signal) and disrupted mitochondrial localization in wild type oocytes, they did not significantly affect the localization of mitochondria in PADI6-null oocytes. These results indicate that while PADI6-null oocytes appear to have an active MT network (as demonstrated by the hyperpolymerized MTs), organelle redistribution in these oocytes is defective. The inability of organelles to be “pulled along” by MTs in mutant oocytes in these

experiments suggests that the tubulin-containing PADI6/CPL complex plays a role in mediating the association of ER and mitochondria with cytoplasmic MTs during oocyte maturation.

Levels of Acetylated Tubulin Are Dramatically Reduced in the Cytoplasm of *Padi6*-null Oocytes

Regulation of ATP-ase dependent MT motor activity is mediated by a wide range of factors including MT-associated proteins, cell cycle regulatory factors, and, more recently, tubulin acetylation (Barlan and Gelfand, 2010). In somatic cells, tubulin acetylation specifically occurs on lysine 40 of α-tubulin following MT assembly and this post-translational modification was previously documented to be abundantly represented in stable microtubules (Hammond et al., 2008). Interestingly, tubulin acetylation has also recently been found by several groups to play a critical role in the trafficking of cellular cargo by both dynein and kinesin (Cambray-Deakin et al., 1988; Chen et al., 2010). Further, a very recent report has demonstrated that ER movement occurs along stable acetylated MTs in somatic cells. These investigators also show that mitochondria are found to be directly associated with the ER on acetylated MT (Friedman et al., 2010). In mammalian oocytes, acetylated tubulin has also previously been associated with stable microtubules at the spindle poles, however, a potential role in cytoplasmic organelle redistribution has not been previously investigated (Schatten et al., 1985).

Given these observations, and our observed links between tubulin and the CPLs, we next investigated whether acetylated tubulin might be altered in PADI6-null oocytes, thus providing a potential mechanistic explanation for the observed organelle distribution defects. We carried out IIF and western blot analysis on oocytes using anti-acetylated tubulin and found that levels of cytoplasmic acetylated tubulin were reduced in PADI6-null GV and MII-stage oocytes (Figure 5A-D). This apparent decrease in staining was particularly evident in MII-arrested oocytes where almost no signal was observed outside of the meiotic spindle apparatus (Figure 5C). In order to confirm that the cytoplasmic anti-acetylated tubulin signal was specifically due to reactivity with acetylated tubulin, we next *in vitro* matured oocytes with the HDAC inhibitor, trichostatin A (TSA) (Hubbert et al., 2002), and then probed the oocytes with anti-acetylated tubulin. IIF and western analyses found that TSA treatment strongly enhanced the cytoplasmic signal and the appropriately sized band in both wild type and PADI6-null oocytes (Figure 5E-F and Figure S5). These findings indicate that, while PADI6-null oocytes appear to contain normal levels of acetylated tubulin at the meiotic spindle, tubulin acetylation in the oocyte cytoplasm is strongly suppressed (arrows in Figure 5C). Further, these results also support the hypothesis that PADI6 and the CPLs play a key role in facilitating and/or maintaining MT acetylation in the oocyte cytoplasm.

Several potential mechanisms are envisioned by which PADI6 and/or the oocyte lattices could facilitate the formation of stable acetylated microtubules. Given our finding that a subset of alpha tubulin appears to co-localize with PADI6 at the CPLs, our current working hypothesis is that the lattices may function as a nucleating site for the generation of stable microtubules in the oocyte cytoplasm. Further, we predict that as opposed to MTOCs, which mediate MT spindle assembly (Schuh and Ellenberg, 2007), this distinct set of stable microtubules will be found to primarily function in organelle redistribution and possibly other cytoplasmic maturation events. Alternatively, it is also possible that the lattices function as a signaling scaffold that is required for posttranslational modification of cytoplasmic microtubules during the assembly of stable MTs. We are currently carrying out experiments to test these different hypotheses.

Inhibition of the MT Motors, Dynein and Kinesin, Does not Affect Organelle Targeting in *Padi6*-null Oocytes

MT mediated organelle transport is facilitated by molecular motor proteins such as the kinesins, which move along the MT from the minus end to the plus end, and dynein, which moves in the opposite direction (Thaler and Haimo, 1996). We predicted that the observed organelle redistribution defects in PADI6-null oocytes were caused by the inability of organelles to associate with MTs due to a depletion of cytoplasmic acetylated MTs. If this prediction was correct, then one would also predict that kinesin and dynein trafficking would be defective in PADI6-null oocytes since these motors utilize acetylated MT for transport (Reed et al., 2006). To test this hypothesis, we treated wild type and PADI6-null oocytes with vanadate (which inhibits the ATP-ase activity of dyenin) and AMP-PNP (which inhibits the ATP-ase activity of both dynein and kinesin (Harrison and Huebner, 1997) and then investigated the effects of these inhibitors on organelle distribution using ER and Mito Tracker (Figure 5G-H). We found that, while these drugs altered ER and mitochondrial distribution in wild type oocytes as predicted (Figure 5G), these regents did not appear to strongly effect organelle distribution in PADI6-null oocytes (Figure 5H).

Conclusion

This report documents the novel finding that, in addition to its previously described role in ribosomal storage, the cytoplasmic lattices also appears to contain a significant pool of Triton insoluble α-tubulin. Further, our findings also demonstrate that the PADI6/CPL complex plays a critical role in the regulation of MT-mediated organelle positioning and redistribution during oocyte maturation. We then show that tubulin acetylation is strongly depleted in the cytoplasm of PADI6-null oocytes suggesting that the PADI6/CPL complex may regulate organelle positioning and redistribution by facilitating the formation of stable acetylated MTs. While we currently do not fully understand how PADI6 and the CPLs regulate tubulin acetylation, our findings provide new insight into the regulation of MT-mediated trafficking events in mammalian oocytes. Additionally, given that, similar to poor quality human oocytes, *Padi6* mutant oocytes also display a non-polarized diffuse ER and mitochondrial localization pattern, our findings also raise the possibility that the PADI6/CPL complex may function as an important marker for oocyte quality. Finally, given the lack of organelle polarity in PADI6-null oocytes, our findings also suggest that the PADI6 and the CPLs may function as important mediators of cell fate during early development.

Materials and Methods

Animals

The generation of the *Padi6*-deficient mouse strain has been described previously (Esposito et al., 2007). CD-1 mice were purchased from Charles River Laboratories. All mice were housed in the Cornell University Animal Facility (Ithaca, NY) and procedures using these mice were reviewed and approved by the Cornell University Institutional Animal Care and Use Committee. Studies were performed in accordance with the Guiding Principles for the Care and Use of Laboratory Animals.

Oocyte and Embryo Collection and Culture

All experiments were performed using age-matched *Padi6*$^{+/+}$ and *Padi6*$^{-/-}$ females (age 4-7 weeks) primed with gonadotrophins to obtain fully-grown GV oocytes, ovulated oocytes, and embryos. All oocytes and embryos were collected in M2 medium (Sigma) unless otherwise stated. Culture medium was supplemented with 25 mM of milrinone (Sigma) to inhibit GVBD. For in vitro maturation (IVM) and live staining experiments, GV oocytes

were further cultured in MEM-alpha medium (Invitrogen) supplemented with 5% fetal bovine serum (FBS, Atlanta Biologicals).

Immunofluorescence, Scanning Confocal Microscopy, and Co-localization

Indirect immunofluorescence labeling confocal microscopy was undertaken as described previously with a slight modification (Yurttas et al., 2008).For Triton extraction experiments, oocytes and embryos were incubated first for 10 minutes in extraction buffer containing 0.1 M KCl, 20 mM $MgCl_2$, 3 mM EGTA, 20 mM HEPES (pH 6.8), 0.1% Triton X-100 (Sigma), 1x Complete Protease Inhibitor Cocktail (Roche) then rinsed quickly three times in DPBS before fixation in 4% paraformaldehyde (PFA, EM Sciences) in PBS. Guinea pig anti-PADI6 (1:1000) (Wright et al., 2003), mouse anti-α-tubulin (1:1000) (T5168, Sigma), normal guinea pig Ig G (1:1000) (Santa Cruz), normal mouse IgG (1:1000) (Santa Cruz) rabbit-anti-DDX6 (1:500, Bethyl Laboratories), mouse anti-Aurora A kinase (1:200, Abcam), rabbit anti-phospho-histone H3 (ser10) (1:50, Upstate), goat anti-calreticulin (1:20, Santa Cruz), mouse anti-Cytochrome C (1:50, BD Pharmingen), rabbit anti-acetylated H4K5(1:50, Abcam), and mouse anti-acetylated tubulin (1:200, Sigma) antibodies were used. Images were obtained on LSM 510 laser scanning confocal microscope (Carl Zeiss, Germany) equipped with Zen 2007 software for image processing and co-localization analysis. Co-localization coefficient represents the relative number of co-localizing pixels in PADI6 channel or α-tubulin channel as compared to the total number of pixels above threshold. Manders' overlap coefficient indicates an actual overlap of signals, represents the true degree of co-localization. Pearson's correlation coefficient describes the correlation of the intensity distribution between PADI6 and α-tubulin channels.

Human oocytes were obtained for research after informed patient consent under a protocol approved by The New York Presbyterian Hospital-Weill Medical College of Cornell University Institutional Review Board. Mature failed to fertilize human oocytes were fixed in 4% PFA and processed for indirect immunofluorescence labeling confocal microscopy. Images were obtained on LSM 510 confocal microscope (Carl Zeiss, Germany).

Immuno-electron Microscopy

Superovulated oocytes were collected and fixed immediately in 4% paraformaldehyde (PFA) and 0.5% glutaraldehyde (EM Sciences) in PBS buffer for 2 hours. After washing in PBS, oocytes were rapidly dehydrated through an ethanol concentration gradient and embedded in LR White (EM Sciences). Thin sections (60 nm) were cut using a diamond knife (Diatome) on an ultramicrotome (Sorvall MT6000) and placed on nickel grids. For immunostaining, grids were incubated with blocking buffer (EM Sciences) followed by primary antibodies including guinea pig anti-PADI6 (1:50), mouse anti-α-tubulin (1:50, Sigma) or pre-immune sera as negative controls. After incubation, grids were washed and incubated with secondary antibodies containing goat anti-mouse IgG complexed with 10 nm gold (1:100, EM Sciences) and goat anti guinea pig labeled with 6 nm gold (1:100, EM Sciences) followed by washes with 1% Tween 20 in PBS and ddH_2O. Sections were contrast-enhanced using 2% uranyl acetate, washed with ddH_2O, and air-dried. Samples were visualized on a FEI Tecnai T-12 transmission electron microscope (FEI) operated at 120 KV and equipped with iTEM and TIA imaging software.

Immunoprecipitation

GV stage oocytes were isolated from the ovaries of CD1 females and washed with ice-cold PBS before being placed in lysis buffer consisting 0.5% Triton and 1× Complete Protease Inhibitor Cocktail in PBS for 30 minutes on ice. Lysate was centrifuged and supernatants were pre-cleared with pre-imunue serum and protein A Sepharose beads. After clearing, supernatants were then incubated either with guinea pig anti-PADI6 antibody or pre-immune

serum for 2 hours at 4°C and further incubated with protein A Sepharose (GE Healthcare). The immune complex was pelleted, washed, and were resolved by SDS-PAGE and immunoblotted with anti-α-tubulin antibodies, as described below. The blot was then probed with peroxidase-conjugated goat anti-mouse IgG light chain secondary antibody (1:20,000, Jackson ImmunoResearch Laboratories) to reveal tubulin staining.

Electron Microscopy

Electron microscopy (EM) was performed as described elsewhere (Gallicano et al., 1991; Yurttas et al., 2008). Samples were visualized, captured, and stored on a FEI Tecnai T-12 transmission electron microscope (FEI) operated at 120 kV and equipped with iTEM and TIA imaging software.

Immunoblotting

Oocytes were lysed in Laemmli loading buffer and analyzed on SDS-PAGE gel. Proteins were separated at 120 V for 1 20 minutes and then transferred to a PVDF membrane. All blots were blocked with 5% nonfat dry milk in TBS containing 0.1% Tween-20 (TBST, Sigma), washed three times with TBST and incubated with guinea pig anti-PADI6 antibody (1:20,000), mouse anti-α-tubulin (1:8,000, Sigma), mouse anti-acetylated tubulin (1:500, Sigma), and rabbit anti-beta-actin (1:500, Abcam). Blots were then washed and incubated with 1:20,000 dilution of peroxidase-conjugated secondary antibodies (Jackson ImmunoResearch). Immobilon Western HRP Chemiluminescent Substrate (Millipore) was applied to the washed membranes and the film was developed.

In Vitro Culture and Live Staining of Oocytes

For MT and organelle staining, GV oocytes were collected in M2 medium with 25μm milrinone and cultured in MEM alpha plus 5% FBS at 37°C in an atmosphere of 5% CO_2, 5% O_2 and 90% N_2. Oocytes were then stained at different time points for analysis. Briefly, oocytes were cultured in MEM alpha containing 250 nM of MitoTracker Deep Red 633 (Invitrogen), 1 μM of ER-Tracker Red (Invitrogen), 500 nM of Green Tubulin Tracker for 30 minutes at 37°C, 5% CO_2, and 1μg/ml of Hoechst 33342 (Sigma) was added during the last 10 minutes incubation. In the case of drug treatment, 10 μM of taxol (Sigma) was added to the culture medium for 15 minutes prior to the addition of dyes for organelle staining. After incubation, cells were washed and attached to the glass bottom of MatTek culture dishes (Ashland, MA). Digital images were recorded on the Zeiss LSM 510 confocal microscope. In the multicolor labeling experiments, the confocal configuration was set up to avoid the bleed-through of fluorescence dyes.

Meiotic Metaphase-II Spindle Analysis

Analysis of MII spindle MTs was undertaken using published techniques (Kan et al., 2008). Oocytes were incubated with a 1:500 dilution of mouse monoclonal antibody to α-tubulin (Sigma) and 1:500 dilution of anti-PADI6 antibody. Images were scored on a Zeiss LSM 510 scanning confocal microscope using Zen 2007 software.

Morphometric Analysis

Six *Padi6*$^{+/+}$ and six *Padi6*$^{-/-}$ oocytes (originating from two different females per group) were utilized for these studies with 7 images being scored per oocyte. Oocyte images were taken at a magnification of 15370 × using a 1989 grid containing points spaced at 0.5 cm. Morphometry was then performed and the area of each oocyte was determined by counting the number of points that land on the oocytes image. Next, the number of points occupied by each organelle within the oocyte image was counted. Knowing the area of each oocyte section and the area of each organelle, a comparable percent was calculated per organelle.

Data were compiled and analyzed using Microsoft Excel 2003. Comparisons were made using unpaired *t*-test. The threshold of statistical significance was set at $P<0.05$.

Manipulation of MTs and MT Motor Proteins

For the MT perturbation experiments, drugs were prepared in DMSO at high concentrations and then stored at -20°C. Mature oocytes were isolated wild-type and PADI6-null females and incubated for 45min-1 hour in MEM-alpha media supplemented with DMSO, Taxol (10μM), nacodazole (20μg/ml), or vinblastine (10 μg/ml), respectively. The live oocytes were then incubated with Mito or ER tracker and imaged by confocal microscopy. For the motor protein inhibition experiments, GV-stage oocytes were cultured with DMSO, sodium orthovanadate (500 μM), or AMP-PNP (2mM) for 3 hours followed by live staining and imaging as described above. For the TSA treatment experiments, GV-stage oocytes were cultured in MEM-alpha media supplemented with 5% FBS and TSA (100nM) for ~18 hours at 37°C in an atmosphere of 5% CO_2, 5% O_2 and 90% N_2. The in vitro matured oocytes were then collected for IIF or Western blot analysis.

Statistical Analysis

All experiments used for quantification were repeated at least three times. Data were compiled and analyzed using Microsoft Excel 2003. Comparisons were made for the length of spindle, the width of spindle poles, the width of spindle equator, the width of chromosome alignment, the distance of spindle to cortex in *Padi6* wild-type versus mutant mature oocytes, and the polyspermic fertilization using unpaired *t*-test. The threshold of statistical significance was set at $P<0.05$.

Research Highlights

- Alpha tubulin is associated with PADI6 at the oocyte cytoplasmic lattices.
- PADI6 and the oocyte lattices play a critical role in the redistribution of mitochondria and endoplasmic reticulum during oocyte maturation.
- Organelles are diffusely distributed in PADI6-null oocytes and appear to be dissociated from microtubules.
- PADI6-null oocytes appear to lack stable acetylated cytoplasmic microtubules.

Supplementary Material

Refer to Web version on PubMed Central for supplementary material.

Acknowledgments

This research was supported by NICHD grants RO1 38353 and RO3 522241 (S.A.C.). We thank John Eppig and Karen Wigglesworth for their technical assistance with oocyte culture; Lynne Anguish and John Grazul for their technical support in TEM. We also thank Carmen Williams (NIEHS) for generous gift of anti-calreticulin antibody.

References

Barlan K, Gelfand VI. Intracellular Transport: ER and Mitochondria Meet and Greet along Designated Tracks. Curr Biol. 2010; 20:R845–847. [PubMed: 20937470]

Calarco-Gillam PD, Siebert MC, Hubble R, Mitchison T, Kirschner M. Centrosome development in early mouse embryos as defined by an autoantibody against pericentriolar material. Cell. 1983; 35:621–629. [PubMed: 6652679]

Cambray-Deakin MA, Robson SJ, Burgoyne RD. Colocalisation of acetylated microtubules, glial filaments, and mitochondria in astrocytes in vitro. Cell Motil Cytoskeleton. 1988; 10:438–449. [PubMed: 3052874]

Chen S, Owens GC, Makarenkova H, Edelman DB. HDAC6 regulates mitochondrial transport in hippocampal neurons. PLoS One. 2010; 5:e10848. [PubMed: 20520769]

Combelles CM, Albertini DF. Microtubule patterning during meiotic maturation in mouse oocytes is determined by cell cycle-specific sorting and redistribution of gamma-tubulin. Dev Biol. 2001; 239:281–294. [PubMed: 11784035]

Elinson RP, Rowning B. A transient array of parallel microtubules in frog eggs: potential tracks for a cytoplasmic rotation that specifies the dorso-ventral axis. Dev Biol. 1988; 128:185–197. [PubMed: 3289985]

Esposito G, Vitale AM, Leijten FP, Strik AM, Koonen-Reemst AM, Yurttas P, Robben TJ, Coonrod S, Gossen JA. Peptidylarginine deiminase (PAD) 6 is essential for oocyte cytoskeletal sheet formation and female fertility. Mol Cell Endocrinol. 2007; 273:25–31. [PubMed: 17587491]

FitzHarris G, Marangos P, Carroll J. Cell cycle-dependent regulation of structure of endoplasmic reticulum and inositol 1,4,5-trisphosphate-induced Ca2+ release in mouse oocytes and embryos. Mol Biol Cell. 2003; 14:288–301. [PubMed: 12529444]

FitzHarris G, Marangos P, Carroll J. Changes in endoplasmic reticulum structure during mouse oocyte maturation are controlled by the cytoskeleton and cytoplasmic dynein. Dev Biol. 2007; 305:133–144. [PubMed: 17368610]

Flemr M, Ma J, Schultz RM, Svoboda P. P-body loss is concomitant with formation of a messenger RNA storage domain in mouse oocytes. Biol Reprod. 2010; 82:1008–1017. [PubMed: 20075394]

Friedman JR, Webster BM, Mastronarde DN, Verhey KJ, Voeltz GK. ER sliding dynamics and ER-mitochondrial contacts occur on acetylated microtubules. J Cell Biol. 2010; 190:363–375. [PubMed: 20696706]

Gallicano GI, McGaughey RW, Capco DG. Cytoskeleton of the mouse egg and embryo: reorganization of planar elements. Cell Motil Cytoskeleton. 1991; 18:143–154. [PubMed: 2013110]

Gallicano GI, McGaughey RW, Capco DG. Cytoskeletal sheets appear as universal components of mammalian eggs. J Exp Zool. 1992; 263:194–203. [PubMed: 1500884]

Gard DL. Organization, nucleation, and acetylation of microtubules in Xenopus laevis oocytes: a study by confocal immunofluorescence microscopy. Dev Biol. 1991; 143:346–362. [PubMed: 1991557]

Hammond JW, Cai D, Verhey KJ. Tubulin modifications and their cellular functions. Curr Opin Cell Biol. 2008; 20:71–76. [PubMed: 18226514]

Harrison RE, Huebner E. Unipolar microtubule array is directly involved in nurse cell-oocyte transport. Cell Motil Cytoskeleton. 1997; 36:355–362. [PubMed: 9096957]

Hirokawa N, Noda Y, Okada Y. Kinesin and dynein superfamily proteins in organelle transport and cell division. Curr Opin Cell Biol. 1998; 10:60–73. [PubMed: 9484596]

Hsieh CS, Chen SU, Lee YW, Yang YS, Sun CK. Higher harmonic generation microscopy of in vitro cultured mammal oocytes and embryos. Opt Express. 2008; 16:11574–11588. [PubMed: 18648479]

Hubbert C, Guardiola A, Shao R, Kawaguchi Y, Ito A, Nixon A, Yoshida M, Wang XF, Yao TP. HDAC6 is a microtubule-associated deacetylase. Nature. 2002; 417:455–458. [PubMed: 12024216]

Kan R, Sun X, Kolas NK, Avdievich E, Kneitz B, Edelmann W, Cohen PE. Comparative analysis of meiotic progression in female mice bearing mutations in genes of the DNA mismatch repair pathway. Biol Reprod. 2008; 78:462–471. [PubMed: 18057311]

Kim B, Kan R, Anguish L, Nelson LM, Coonrod SA. Potential role for MATER in cytoplasmic lattice formation in murine oocytes. PLoS One. 2010; 5:e12587. [PubMed: 20830304]

Lane JD, Allan VJ. Microtubule-based endoplasmic reticulum motility in Xenopus laevis: activation of membrane-associated kinesin during development. Mol Biol Cell. 1999; 10:1909–1922. [PubMed: 10359605]

Lehtonen E. A monoclonal antibody against mouse oocyte cytoskeleton recognizing cytokeratin-type filaments. J Embryol Exp Morphol. 1985; 90:197–209. [PubMed: 2422311]

Lessman CA. Germinal vesicle migration and dissolution in Rana pipiens oocytes: effect of steroids and microtubule poisons. Cell Differ. 1987; 20:239–251. [PubMed: 2884043]

Lessman CA, Kim H. Soluble tubulin complexes in oocytes of the common leopard frog, Rana pipiens, contain gamma-tubulin. Mol Reprod Dev. 2001; 60:128–136. [PubMed: 11550276]

Liu J, Lessman CA. Soluble tubulin complexes, gamma-tubulin, and their changing distribution in the zebrafish (Danio rerio) ovary, oocyte and embryo. Comp Biochem Physiol B Biochem Mol Biol. 2007; 147:56–73. [PubMed: 17293149]

Maro B, Kubiak J, Gueth C, De Pennart H, Houliston E, Weber M, Antony C, Aghion J. Cytoskeleton organization during oogenesis, fertilization and preimplantation development of the mouse. Int J Dev Biol. 1990; 34:127–137. [PubMed: 2203452]

Maro B, Verlhac MH. Polar body formation: new rules for asymmetric divisions. Nat Cell Biol. 2002; 4:E281–283. [PubMed: 12461532]

Mehlmann LM, Terasaki M, Jaffe LA, Kline D. Reorganization of the endoplasmic reticulum during meiotic maturation of the mouse oocyte. Dev Biol. 1995; 170:607–615. [PubMed: 7649387]

Minshall N, Standart N. The active form of Xp54 RNA helicase in translational repression is an RNA-mediated oligomer. Nucleic Acids Res. 2004; 32:1325–1334. [PubMed: 14982957]

Pepling ME, Wilhelm JE, O'Hara AL, Gephardt GW, Spradling AC. Mouse oocytes within germ cell cysts and primordial follicles contain a Balbiani body. Proc Natl Acad Sci U S A. 2007; 104:187–192. [PubMed: 17189423]

Reed NA, Cai D, Blasius TL, Jih GT, Meyhofer E, Gaertig J, Verhey KJ. Microtubule acetylation promotes kinesin-1 binding and transport. Curr Biol. 2006; 16:2166–2172. [PubMed: 17084703]

Ruiz-Meana M, Abellan A, Miro-Casas E, Agullo E, Garcia-Dorado D. Role of sarcoplasmic reticulum in mitochondrial permeability transition and cardiomyocyte death during reperfusion. Am J Physiol Heart Circ Physiol. 2009; 297:H1281–1289. [PubMed: 19684187]

Saskova A, Solc P, Baran V, Kubelka M, Schultz RM, Motlik J. Aurora kinase A controls meiosis I progression in mouse oocytes. Cell Cycle. 2008; 7:2368–2376. [PubMed: 18677115]

Schatten G, Simerly C, Schatten H. Microtubule configurations during fertilization, mitosis, and early development in the mouse and the requirement for egg microtubule-mediated motility during mammalian fertilization. Proc Natl Acad Sci U S A. 1985; 82:4152–4156. [PubMed: 3889922]

Schroeder MM, Gard DL. Organization and regulation of cortical microtubules during the first cell cycle of Xenopus eggs. Development. 1992; 114:699–709. [PubMed: 1618137]

Schuh M, Ellenberg J. Self-organization of MTOCs replaces centrosome function during acentrosomal spindle assembly in live mouse oocytes. Cell. 2007; 130:484–498. [PubMed: 17693257]

Shubeita GT, Tran SL, Xu J, Vershinin M, Cermelli S, Cotton SL, Welte MA, Gross SP. Consequences of motor copy number on the intracellular transport of kinesin-1-driven lipid droplets. Cell. 2008; 135:1098–1107. [PubMed: 19070579]

Swain JE, Ding J, Brautigan DL, Villa-Moruzzi E, Smith GD. Proper chromatin condensation and maintenance of histone H3 phosphorylation during mouse oocyte meiosis requires protein phosphatase activity. Biol Reprod. 2007; 76:628–638. [PubMed: 17182892]

Swain JE, Ding J, Wu J, Smith GD. Regulation of spindle and chromatin dynamics during early and late stages of oocyte maturation by aurora kinases. Mol Hum Reprod. 2008; 14:291–299. [PubMed: 18353803]

Thaler CD, Haimo LT. Microtubules and microtubule motors: mechanisms of regulation. Int Rev Cytol. 1996; 164:269–327. [PubMed: 8575892]

Tutuncu L, Stein P, Ord TS, Jorgez CJ, Williams CJ. Calreticulin on the mouse egg surface mediates transmembrane signaling linked to cell cycle resumption. Dev Biol. 2004; 270:246–260. [PubMed: 15136153]

Van Blerkom J. Microtubule mediation of cytoplasmic and nuclear maturation during the early stages of resumed meiosis in cultured mouse oocytes. Proc Natl Acad Sci U S A. 1991; 88:5031–5035. [PubMed: 2052585]

Van Blerkom J, Runner MN. Mitochondrial reorganization during resumption of arrested meiosis in the mouse oocyte. Am J Anat. 1984; 171:335–355. [PubMed: 6517035]

Wassarman PM, Josefowicz WJ. Oocyte development in the mouse: an ultrastructural comparison of oocytes isolated at various stages of growth and meiotic competence. J Morphol. 1978; 156:209–235. [PubMed: 642015]

Wright PW, Bolling LC, Calvert ME, Sarmento OF, Berkeley EV, Shea MC, Hao Z, Jayes FC, Bush LA, Shetty J, Shore AN, Reddi PP, Tung KS, Samy E, Allietta MM, Sherman NE, Herr JC, Coonrod SA. ePAD, an oocyte and early embryo-abundant peptidylarginine deiminase-like protein that localizes to egg cytoplasmic sheets. Dev Biol. 2003; 256:73–88. [PubMed: 12654293]

Xu F, Mukhopadhyay S, Sehgal PB. Live cell imaging of interleukin-6-induced targeting of “transcription factor” STAT3 to sequestering endosomes in the cytoplasm. Am J Physiol Cell Physiol. 2007; 293:C1374–1382. [PubMed: 17670892]

Yisraeli JK, Sokol S, Melton DA. A two-step model for the localization of maternal mRNA in Xenopus oocytes: involvement of microtubules and microfilaments in the translocation and anchoring of Vg1 mRNA. Development. 1990; 108:289–298. [PubMed: 2351071]

Yurttas P, Vitale AM, Fitzhenry RJ, Cohen-Gould L, Wu W, Gossen JA, Coonrod SA. Role for PADI6 and the cytoplasmic lattices in ribosomal storage in oocytes and translational control in the early mouse embryo. Development. 2008; 135:2627–2636. [PubMed: 18599511]

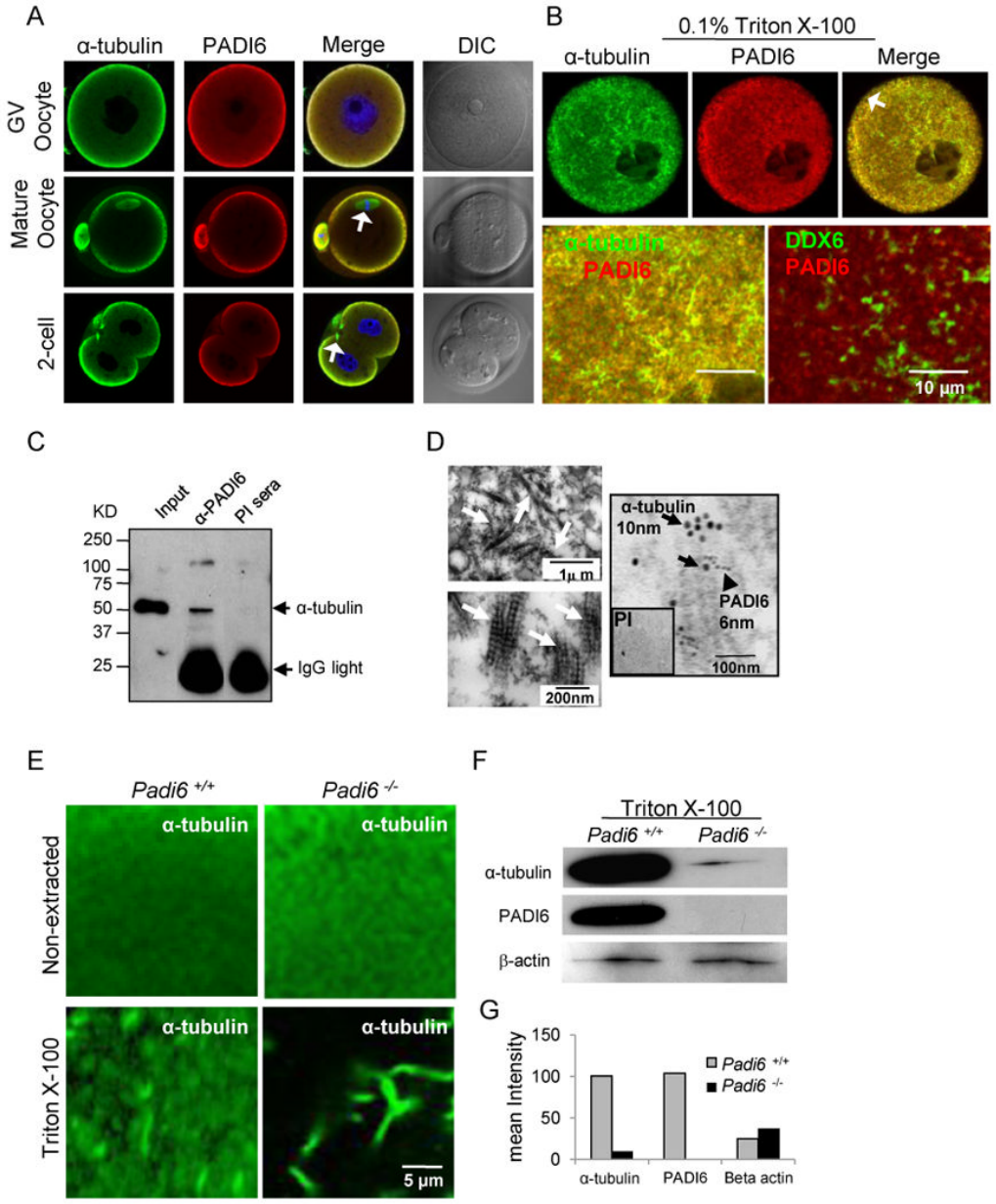

Figure 1. Co-localization and interaction of α-tubulin and PADI6 in murine GV oocytes, mature oocytes, and early embryos

(A-B) Co-localization of α-tubulin and PADI6 by confocal microscopy before (A) and after (B) treatment with 0.1% of Triton X-100 to release soluble proteins. PADI6 and α-tubulin co-localization is highlighted in merged images. Spindle MTs are indicated by white arrows in panel A. Cortical region is indicated by arrow in panel B. The co-localization of DDX6 and PADI6 serves as a control. (C) Immunoprecipitation of α-tubulin from oocyte extracts using anti-PADI6 antibodies. PI = PADI6 pre-immune sera. (D) Ultra-structure of cytoplasmic lattices (CPLs) and co-localization of α-tubulin and PADI6 at the CPLs by immuno-EM. CPL structures are indicated by white arrows in upper (low magnification) and lower (high magnification) left TEM images and are presented here for reference. Immuno-EM image (right panel) with α-tubulin and PADI6-coated gold particles indicated by black arrows and arrow head, respectively. Inset shows PADI6 pre-immune sera. (E) IIF-confocal

analysis of tubulin localization and levels in wild-type and *Padi6*-null oocytes prior to and following extraction with Triton X-100. (F) Western blot analysis of α-tubulin and PADI6 levels in the insoluble pellet of wild type and *Padi6*-null oocytes following extraction with Triton. (G) Staining intensity of α-tubulin bands from wild-type and *Padi6*-null oocytes in Figure F. See also Figure S1, S2 and Table S1.

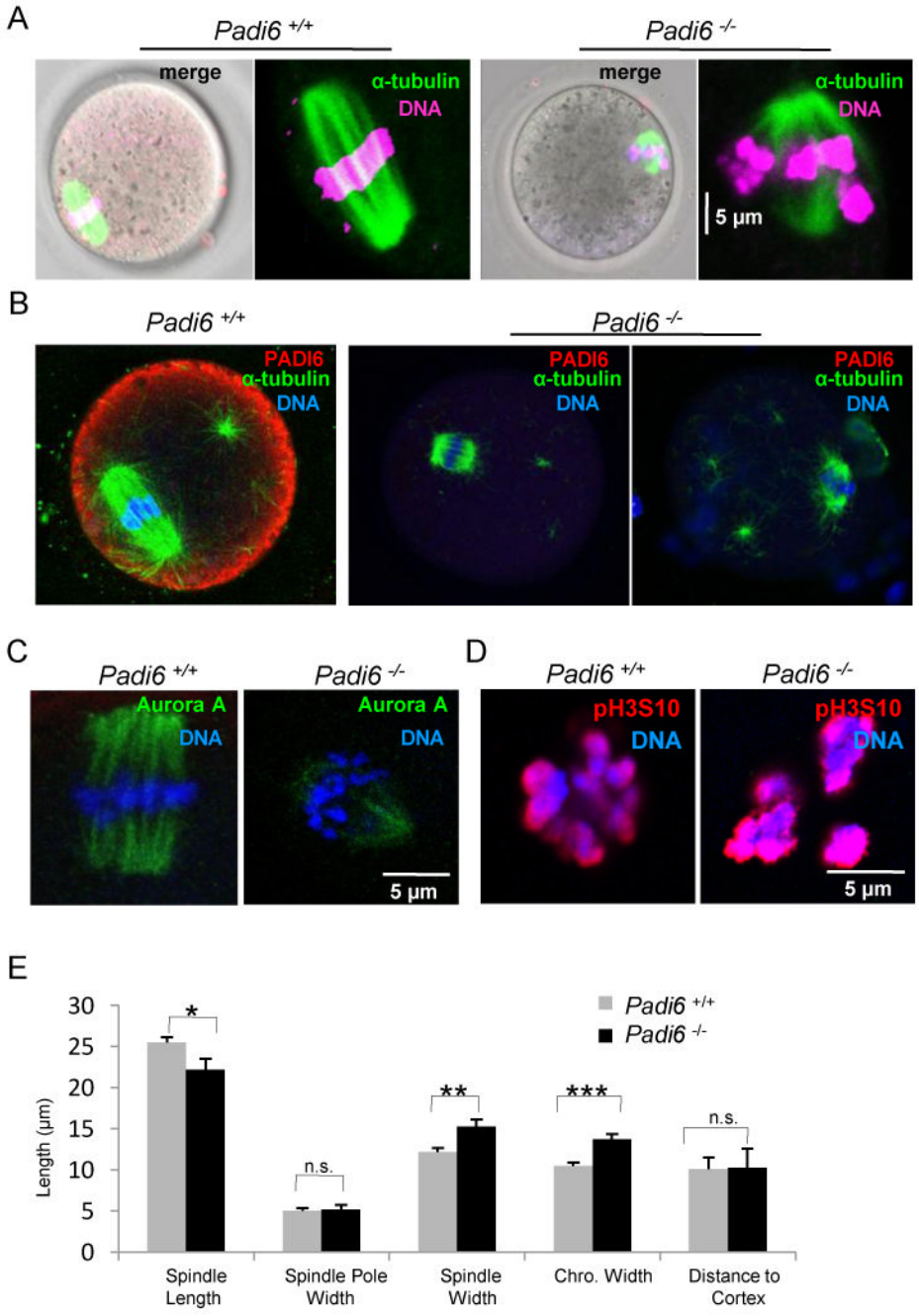

Figure 2. Abnormal meiotic spindle configuration in mature *Padi6*-null oocytes

(A) Spindle MT structure in live oocytes. MTs and DNA were stained with Oregon green 488 Taxol and Hoechst 33342 (magenta), respectively. (B) PFA-fixed oocytes were stained with antibodies to α-tubulin (green) and PADI6 (red). (C) Localization of Aurora kinase A (green) on spindles from *Padi6* wild-type and mutant oocytes. (D) Same as (C) except oocytes were stained with anti-phospho-histone H3 Ser10 antibody (red). (E) Measurement of spindle apparatus from *Padi6* wild-type and mutant oocytes. Chro., chromosome; *, $P < 0.05$; **, $P < 0.001$; ***, $P < 0.0001$; n.s., not significant. Numbers are average ± SEM.

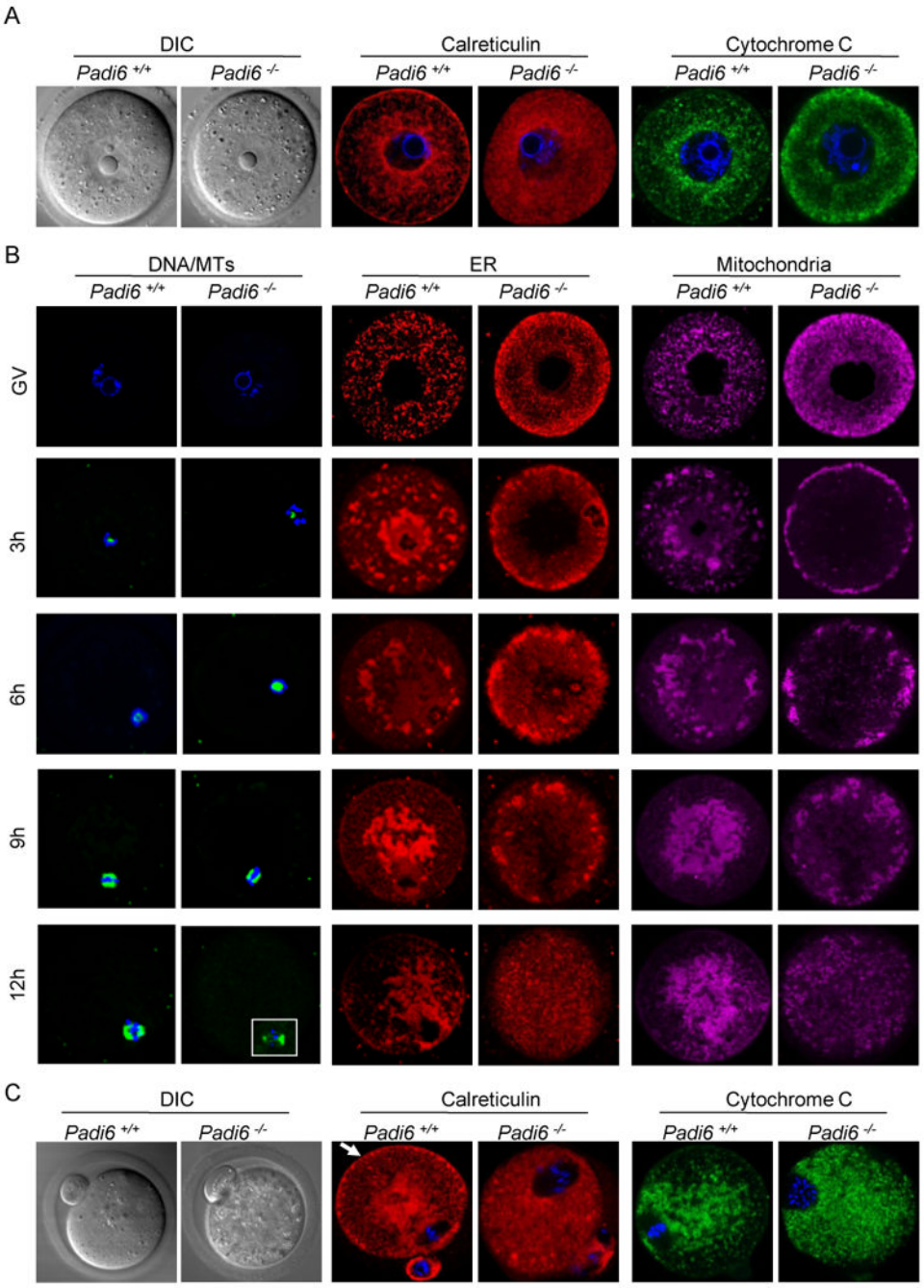

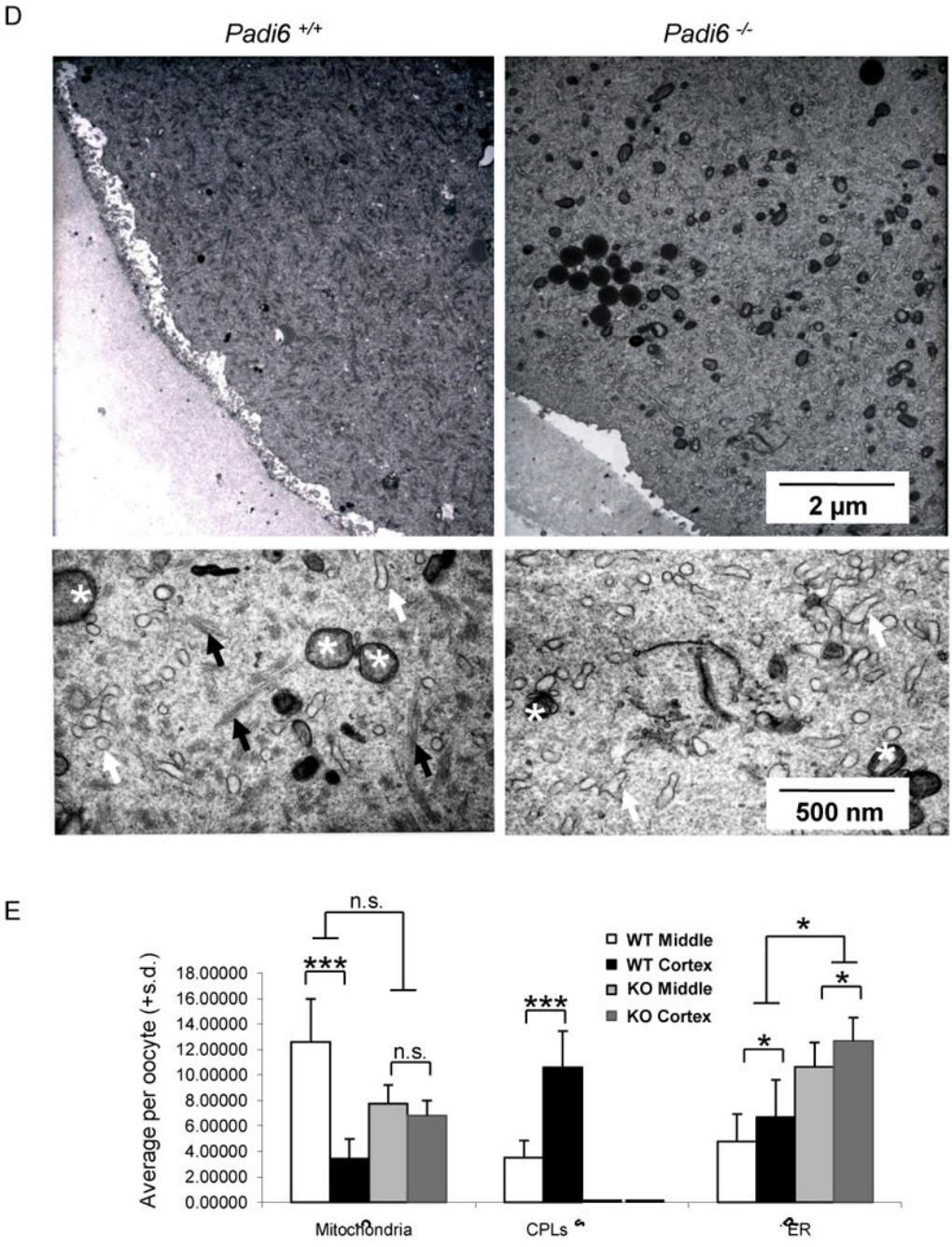

Figure 3. Endoplasmic reticulum (ER) and mitochondrial positioning and redistribution during maturation is altered in *Padi6*-null oocytes

(A) ER and mitochondria localization in GV-stage PFA-fixed oocytes following staining with antibodies to calreticulin (red) and Cytochrome C (green). DIC, differential interference contrast. (B) Time course of organelle redistribution during oocyte maturation. DNA was stained using Hoechst 33342 (blue) and MT was stained with Oregon green 488 Taxol. ER and mitochondria were stained with ER tracker and Mito Tracker, respectively. Oocytes were collected at 3-hour intervals during in vitro culture, fixed, prepared for IIF and imaged by confocal microscopy. (C) Organelle localization in ovulated oocytes recovered from oviducts at 13 hours post hCG and prepared as in (A). Arrow indicates cortical ER

aggregates. (D) TEM images of the metaphase II-arrested wild-type and *Padi6*-null oocyte cortex. The lower panels in (D) are high magnification images. ER and mitochondria are indicated by white arrows and asterisks, respectively. CPLs are indicated by black arrows. (E) Morphometric analyses of CPLs and organelles in the cortical and middle region of wild-type and *Padi6*-null oocytes. *, $P < 0.05$; ***, $P < 0.0001$; n.s., not significant. Numbers are mean ± S.D. of percentage per oocyte. See also Movie S1 and S2.

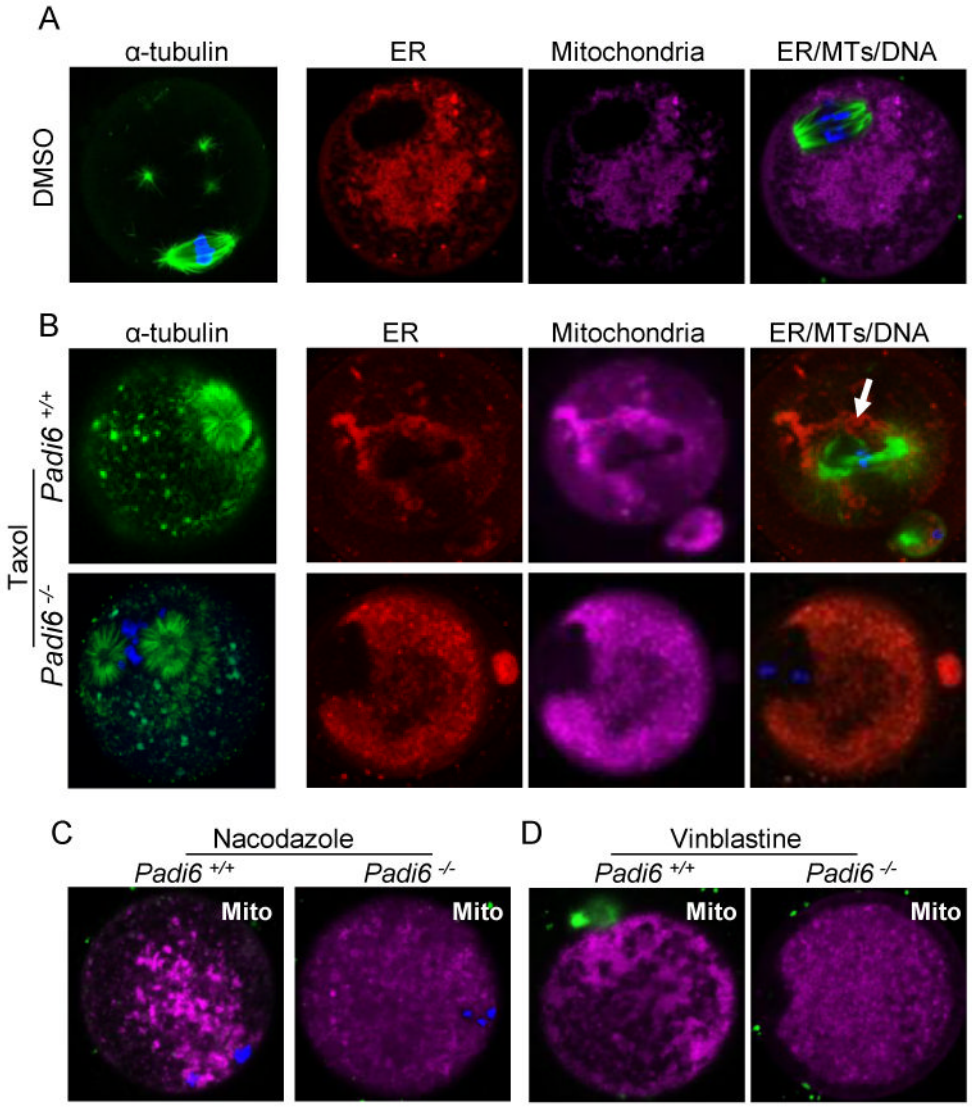

Figure 4. Alteration of MT polymerization does not induce organelle redistribution in *Padi6*-null oocytes

MTs were stained using an anti-α-tubulin antibody in PFA-fixed oocytes while the ER and mitochondria were stained using ER Tracker (red), Mito Tracker (magenta). (A) Control experiment documenting the localization of MTs, ER, and mitochondria in wild type MII-arrested oocytes following DMSO treatment. (B) Localization of MTs, ER and mitochondria in wild type and PADI6-null oocytes following taxol treatment. Arrow indicates taxol-induced organelle clustering around the enlarged wild-type oocyte spindle apparatus. (C) Distribution of mitochondria in wild type and PADI6-null oocytes following nocodazole treatment. (D) Same as (C) except oocytes were pretreated with vinblastine. Mitochondria in (C) and (D) were visualized using Mito Tracker. All oocytes were stained with Hoechst 33342 (blue) to visualize DNA. See also Figure S4.

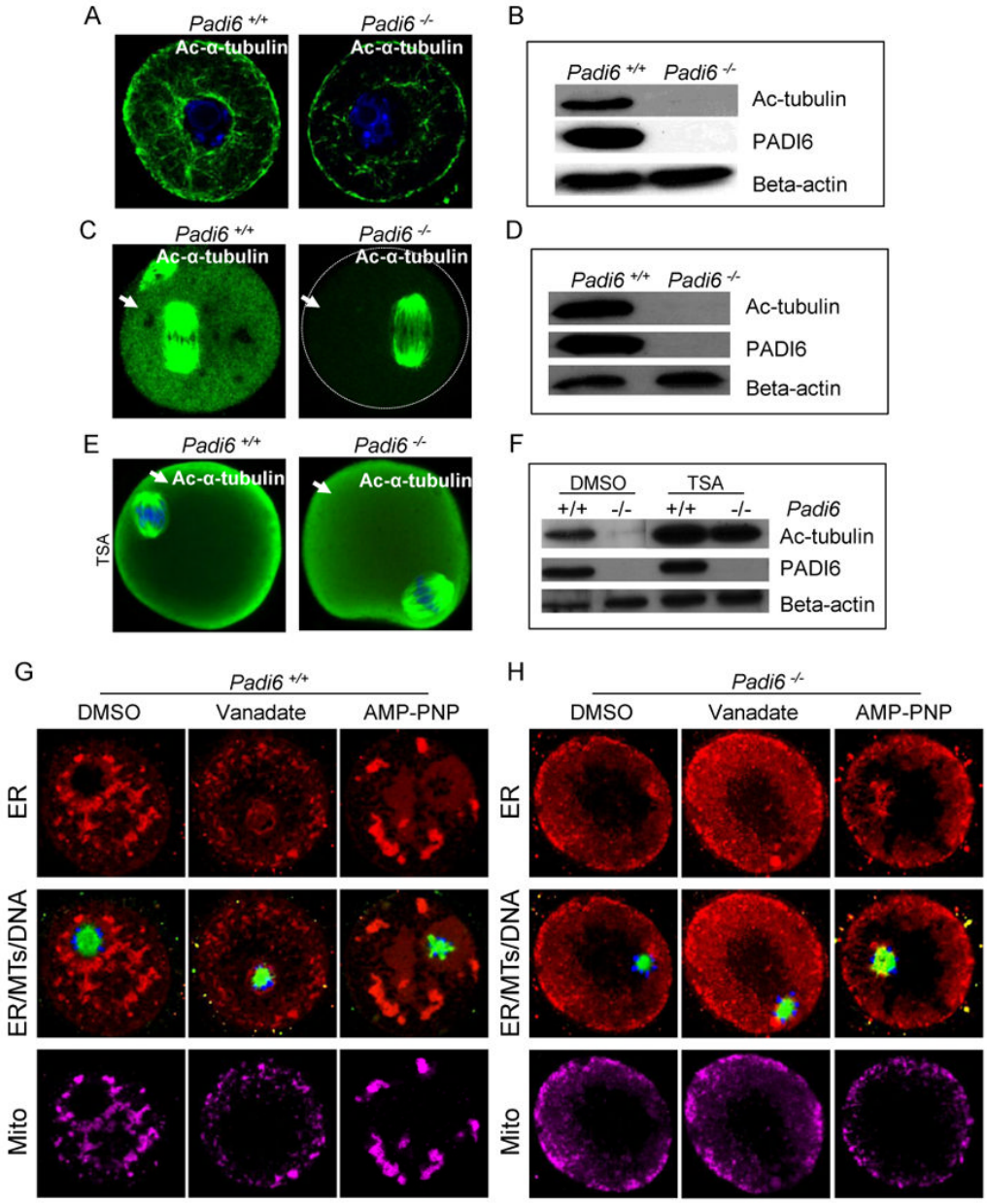

Figure 5. *Padi6*-null oocytes display reduced levels of cytoplasmic acetylated α-tubulin and treatment of these oocytes with MT motor inhibitors does not affect organelle distribution

(A-F) Confocal IIF and western blot analysis of acetylated α-tubulin localization and levels in wild-type and *Padi6*-null GV-stage (A-B), MII-arrested oocytes (C-D), and TSA-treated *in vitro* matured oocytes (E-F). Cytoplasmic acetylated tubulin was indicated by arrows. (G-H) Effect of MT motor inhibitors on organelle distribution in oocytes. *Padi6* wild-type (G) and mutant (H) GV-stage oocytes were cultured with the MT motor inhibitors, vanadate or AMP-PNP, for 3 hours, stained with Tubulin Tracker (green), ER Tracker (red), Mito Tracker (magenta), and Hoechst 33342 (blue), and imaged by confocal microscopy. See also Figure S5.